Discover Applied Sciences

Research

Multifunctional nanorobot system in precise evaluation and manipulation of virus capsid

Yuxuan Xue[1] · Yichen Wang[1] · Xinyu Liu[1] · Jianfeng Lin[1] · Zhiyong Sun[2] · Jiangcheng Chen[3] · Ning Xi[1]

Received: 25 October 2023 / Accepted: 30 April 2024
Published online: 09 May 2024

Abstract
It is imperative to have high adaptive techniques for sensing and manipulating biological targets at the nanoscale. This necessity becomes particularly crucial when dealing with fragile living bio-organisms like viruses, where the expression of capsids is closely linked to viral functions and genome constitution. Therefore, the development of a comprehensive system for dissecting and measuring viruses holds significant implications for the pharmaceutical industry and drug manufacturing. Leveraging the sub-nanometer spatial resolution and controllable tip-cantilever architecture of atomic force microscopy (AFM), a probe-laser system has been integrated as a self-sensing robotic end effector. To address intrinsic challenges in AFM-based robotic systems such as the lack of real-time monitoring, low scanning rates, and nonlinear motion caused by piezoelectric actuators, an augmented reality robotic system has been implemented. This system incorporates stereoscopic vision, a haptic feedback controller, a position recovery scheme, and a real-time force control algorithm. The integration of these components enhances the system's capability to accurately dissect virus capsids. Operators can now perform highly efficient nanoscale tasks with multidimensional perception, utilizing the combination of stereoscopic vision and haptic force control. The position correction during manipulation can achieve a frame rate of over 30 frames per second, imperceptible to the operator, enabling closed-loop operation control. By adopting the proposed nanorobotic system in virology studies, it becomes possible to achieve accurate manipulation and dissection of SARS-CoV-2 pseudovirus capsids, and derive multi-parametric properties such as structural integrity, protein fragment thickness, and adhesive forces. The established nanobot system and experimental results serve as a guiding platform for high-accuracy evaluation in drug manufacturing development.

Keywords Nanorobot · Sars-Cov-2 · Nanosurgery · AFM · Mechanical behavior

Supplementary Information The online version contains supplementary material available at https://doi.org/10.1007/s42452-024-05934-x.

✉ Yuxuan Xue, xueyuxuan@connect.hku.hk; ✉ Jiangcheng Chen, jiangcheng.0502@163.com; ✉ Ning Xi, xining@hku.hk; Yichen Wang, easonwyc@connect.hku.hk; Xinyu Liu, liuxinyu@connect.hku.hk; Jianfeng Lin, jianflin@hku.hk; Zhiyong Sun, sunzy@iim.ac.cn | [1]Department of Industrial and Manufacturing Systems Engineering, The University of Hong Kong, Pokfulam, Hong Kong, China. [2]The Institute of Intelligent Machines, Hefei Institute of Physical Science, CAS, Hefei 230031, China. [3]Shenzhen Academy of Robotics, Shenzhen, Guangdong, China.

1 Introduction

Viruses play a significant role in human daily lives, primarily as infectious agents causing illnesses. The global impact of the COVID-19 pandemic has been devastating, highlighting the crucial need for effective disinfection methods for SARS-CoV-2 [1]. Spherical-shaped viruses typically consist of a protein shell, a viral genome, and spikes attached to the capsid's penton structure [2]. Various approaches, including the use of chemical reagents and germicidal irradiation, have been developed for virus disinfection [3]. However, viruses can also be employed in beneficial applications. Viruses and viral shells can serve as nano scaffolds or nanoreactors for transportation, catalysis, and even cancer treatment [4, 5]. By investigating the structural information and mechanical properties of viruses, their functions can be better understood, particularly through the disassembly of the virus, which provides insights into the molecular structures of capsid protein subunits [6]. Nevertheless, there is a need for a platform that enables dynamic in-situ manipulation and evaluation of viruses, particularly with simultaneous measurements of their mechanical behavior under controlled external excitation.

The advancement of microscopy and automation technology has facilitated extensive investigations into the inspection and manipulation of nanoscale entities, ranging from bioorganisms to the level of DNA [7]. Compared with other nanoscale research tools, such as scanning electron microscopy and transmission electron microscopy that require extra treatment to samples, atomic force microscopy (AFM), which relies on its contact-based mechanism, could directly image the high-resolution topography of virus without altering the situation of targets [8]. AFM-based nanorobotics stand out in a plethora of domains, including biological research, ultra-precision manufacturing, and rapid imaging systems, offering unparalleled precision in nanoscale operations [9–11]. Observing the dynamic responses of viruses to external stimuli via AFM can yield a more profound comprehension of the assembly processes of viral proteins and capsomers into highly ordered structures [12, 13]. Moreover, AFM-based robotic systems introduce an innovative disinfection method by dismantling the physical constructs of viruses through controlled excitations [14].

In AFM, a minuscule probe situated at the apex of a cantilever spring interacts with the sample. The feedback control loop fine-tunes the actuator's motion to achieve nanoscale resolution topography [15]. Beyond imaging, the probe functions similarly to the robotic end-effector, capable of manipulating nanoscale objects and performing lithography on the sample surface [16]. During such manipulations, the AFM nanorobot utilizes its positioning sensors to accurately move the probe, imaging specific areas and reconstructing a local map for reference [17, 18]. Task space positioning capabilities are vital for AFM, as they identify errors between desired operational outputs and actual motions during manipulation and scanning [19]. Despite its ability to produce images with nanoscale resolution, achieving nanometer localization precision is challenging due to system uncertainties, such as uncompensated nonlinearity and thermal drift, which can cause image shifts and distortions over extended capture and operation times. Consequently, positioning errors-stemming from the systematically uncertain distance between the AFM tip and the target-can significantly reduce measurement and manipulation efficiency, especially in smaller work areas [20]. Enhancing the operator's experience through teleportation and virtual reality visualization of AFM operations is crucial for accurate manipulations within a more comfortable environment, providing real-time feedback, which is essential for the improvement of delicate nanoscale tasks [21, 22].

To achieve a high degree of precision in AFM-based measurements and manipulations for fragile living biological samples, the positioning and force error must be regulated and adjusted. For instance, when using the stochastic approach to compensate probe's motion, the error distribution must be specified to ensure the reliability [23]. The visual servoing control technique, in which pictures are often used to find landmark in order to estimate its location to conduct closed-loop operations, is a natural method for addressing the task space positioning uncertainty [24]. Even still, The uncertainty estimation methods lack different implementations due to either considering uncertainty properties as location-independent incidents or estimating them using predefined landmarks with specific structure and size, which may not be available in the native ambient for those tasks [25, 26]. This issue hinders the development of local scan algorithms and the control systems that accompany them. Hence, the further development of a local position recovery scheme is still the crucial task for addressing the uncertainties and inherent error in the AFM-based nanorobotic system.

With the above-mentioned purpose, we introduce an AFM-based nanorobot, augmented by a stereoscopic vision system within an augmented reality (AR) framework, to enhance the AFM's capability for adaptive real-time manipulation. We have developed an optimal spiral local scanning technique that, when paired with a force-sensing decision

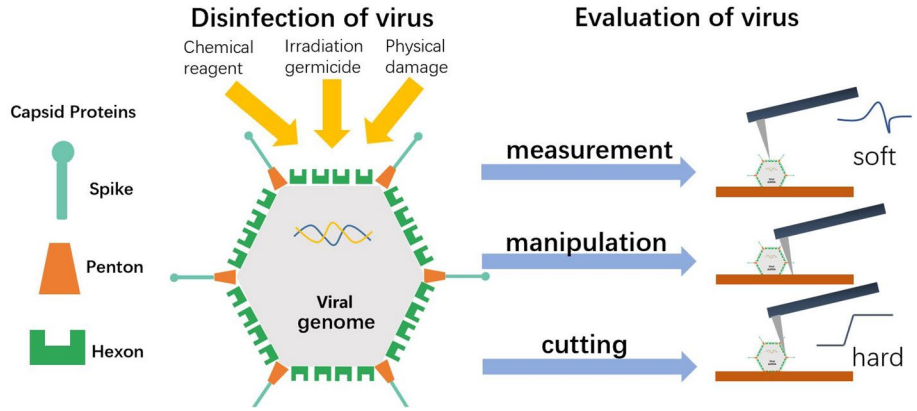

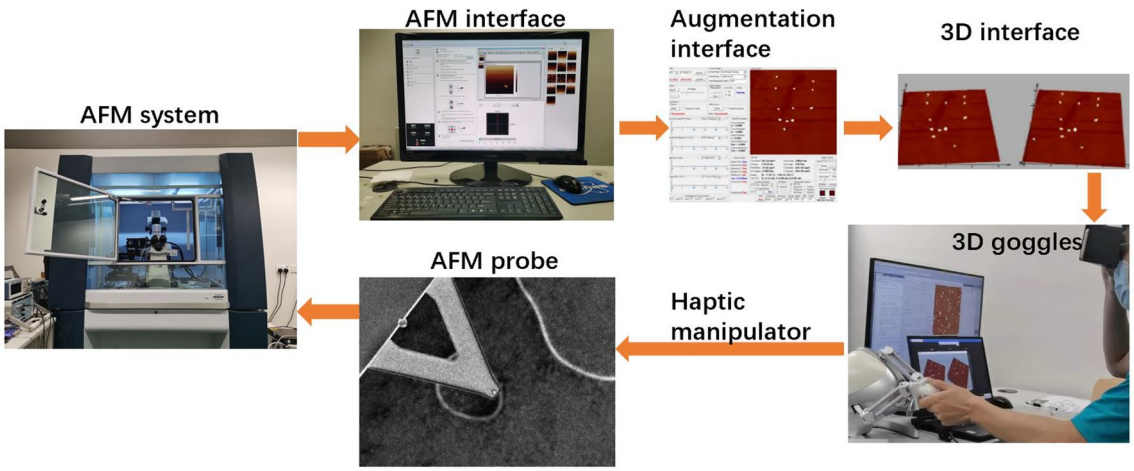

Fig. 1 Schematic of virus capsid under the investigation of nano robot system

Fig. 2 Schematic of the stereoscopic vision-based augmentation reality nanorobotic system

scheme, accurately locates the AFM tip in relation to its surroundings using non-vector space visual servoing control. The system is designed to reconcile the discrepancies between the predetermined desired location and the actual tip location during operation. We also report on the system's performance in engaging with a living pseudo virus resembling SARS-CoV-2. The nanorobot successfully manipulated and disassembled the virus's capsid, examining both its mechanical structure and adhesiveness, as documented by the experimental findings presented in Fig. 1.

2 Stereoscopic vision-based augmentation reality nanorobotic system

Overcoming the intrinsic challenge of lacking real-time visual feedback remains a critical hurdle in nanomanipulation tasks using AFM. Our developed AR system addresses this challenge by dynamically updating the AFM imagery in real-time, informed by spatial and force data acquired during nanomanipulation. The custom-designed software captures signals from the AFM controller through a signal access module, which are then processed by a tailored system and algorithm. Figure 2 illustrates the workings of the AR nanorobotic system. A haptic device is utilized both as a motion controller and a tactile feedback sensor. This augmented setup enables the refresh of the AFM image in the video feed, facilitating a controllable closed-loop manipulation system for objects at the sub-micrometer scale.

To correlate the operation interface motion and force control with the actual AFM signals input, the motion in the operation system $\vec{M}_{GUI}$ and the AFM frame $\vec{M}_{AFM}$ could be determined by following rotational matrix:

$$\vec{M}_{GUI} = R\vec{M}_{AFM} \tag{1}$$

The rotation matrix is stated as following where the ϕ is the scanning attack angle of AFM tips:

$$R = \begin{bmatrix} -cos\phi & sin\phi & 0 \\ -sin\phi & -cos\phi & 0 \\ 0 & 0 & 1 \end{bmatrix} \tag{2}$$

In order to augment the operator's recognition during manipulation tasks, the haptic force generated by the 3D controller is designed to be proportional to the actual force exerted by the AFM probe. The design aims to provide enhanced feedback to the operator, enabling more intuitive and immersive haptic control. The haptic force by 3D controller is stated by:

$$\begin{bmatrix} F_{Hx} & F_{Hy} & F_{Hz} \end{bmatrix}^T = RD \begin{bmatrix} F_{Ax} & F_{Ay} & F_{Az} \end{bmatrix}^T \tag{3}$$

where F_H is the 3d force generated by the controller and F_A is the actual force AFM probe received, the matrix D is the sensitivities for the haptic forces to the AFM probe actual forces which adjusted by the perception of the operator.

$$D = \begin{bmatrix} D_x & 0 & 0 \\ 0 & D_y & 0 \\ 0 & 0 & D_z \end{bmatrix} \tag{4}$$

To augment the operator's perception during manipulation, our system now includes 3D stereoscopic vision. Stereoscopic vision is fundamental for humans to discern three-dimensional space, and it is particularly beneficial for enhancing nanoscale manipulation tasks [27]. We have incorporated real-time stereo visual feedback into our system, taking advantage of the information provided by the AFM probe's imaging feedback and utilizing the generated 3D imagery for subsequent operations. To simulate the operator's binocular vision within this virtual environment, we have positioned two virtual cameras side by side, each sized identically to replicate human eye spacing. The images captured by these cameras are then processed and presented to the operator who, using 3D glasses or a virtual reality headset, experiences separate images for each eye. This setup induces the perception of depth and stereo vision, thereby enhancing the operator's ability to manipulate objects at the nanoscale with greater precision and depth perception (video.S1).

3 Enhanced video rate nanorobotic system by local position recovery scheme

3.1 Framework of local position recovery in task space

AFM Scanner artifacts arise from the nonlinear dynamic behavior of piezoelectric actuators, exhibiting characteristics like non-linearity, creep, and hysteresis. Consequently, the actuator's deformation/displacement is not linearly proportional to the applied voltage. In AFM images, these effects manifest as distortions, particularly noticeable when imaging complex structures. The use of a closed loop scanner could help prevent these artifacts. An instance of image distortion occurs due to non-linearity in the piezo extension. With a tube scanner, the tip follows an arc, resulting in non-linearities in both the lateral and vertical directions [28]. During the operation, when under the time durations at an offset position from the center of the piezoactuator's positioning range, The AFM scanner could lead to substantial precision loss.The creep induced non-linearity could be described with the classic springs and dampers model in Fig. 3 [29].

$$\frac{x(s)}{u(x)} = \frac{1}{k_0} + \sum_{i=1}^{n} \frac{1}{c_i s + k_i} \tag{5}$$

The core of AFM nanorobotic operations lies in the real-time image refreshment facilitated by the local scan scheme, alongside the precise control of the sample-tip position. This control compensates for the motion of nanoscale objects, the AFM tip, and the microenvironment (substrate). This approach significantly reduces scanning errors caused by the non-linearities of the actuators. As shown in Fig. 4, the system utilizes the Bruker AFM (Resolve, Bruker Inc.) and comprises several key components: the AFM scanning unit, the robotic controller, and a user-friendly interface. Enhancements to the AFM system include the integration of peripheral devices such as an upward-facing microscope, a Nikon inverted optical microscope (Eclipse Ti-U), and a CCD camera. These additions provide low-resolution videos of the samples and probes through optical microscopy, enhancing visual accessibility during operations. The real-time control module is equipped with a National Instruments DAQ board (PCI-6361) for data collection and output control signals to the signal access module (Bruker Inc.). Signal transmission is managed through Ethernet using the UDP protocol, facilitating communication

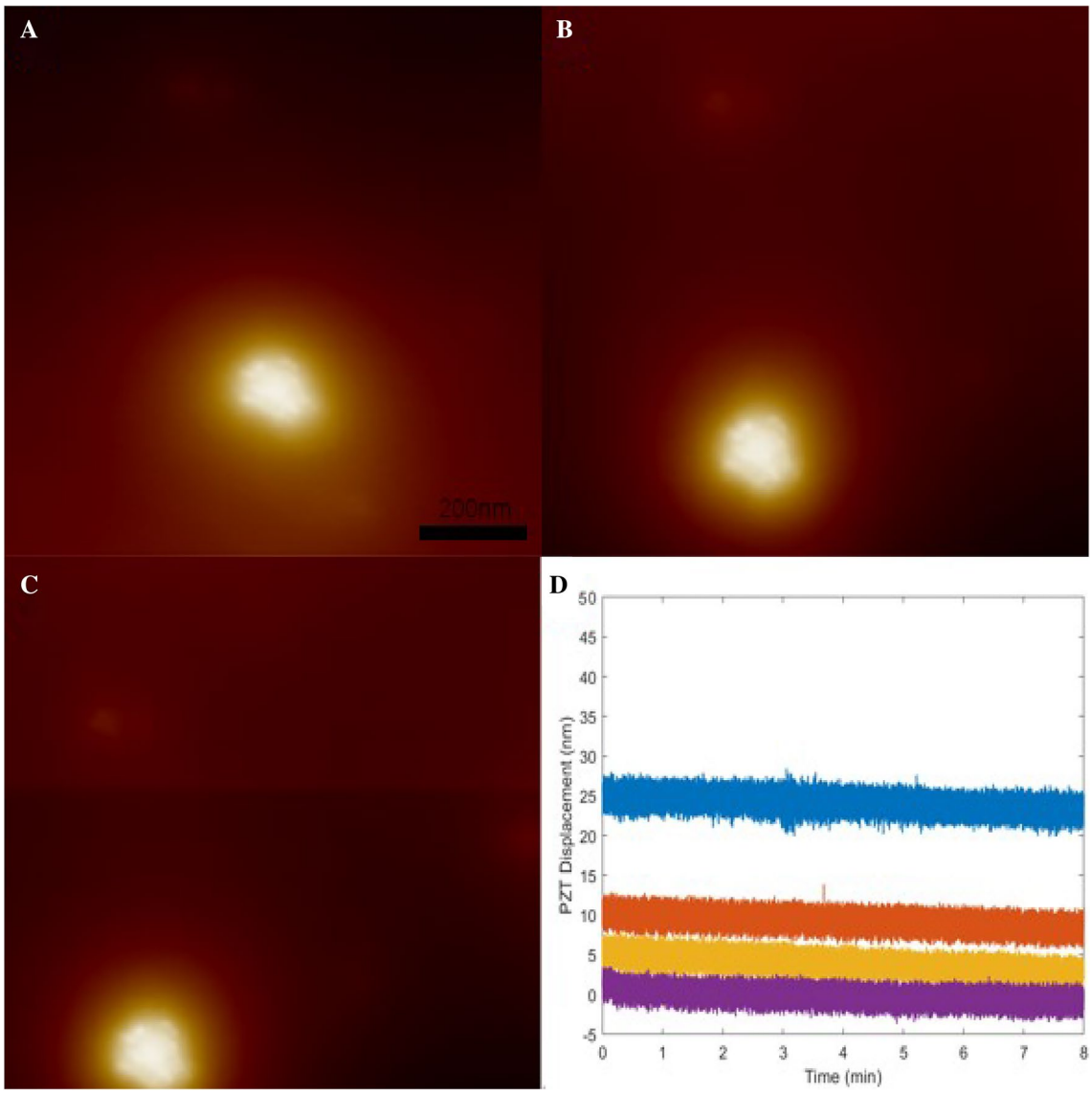

Fig. 3 Scanning Drift of the Sars-Cov-2 capsid during continually operation: **A** 0 hrs; **B** 2 hrs; **C** 4 hrs. **D** X Piezoelectric actuator displacement under different offset

from the user PC to the AFM PC. Additionally, the custom-built PC includes a haptic device (Novint Inc.) and bespoke software 'Nanoviz'. This setup enriches the nanomanipulation process by providing real-time visual feedback and multi-channel signals. The haptic device offers force feedback, enabling operators to feel the force exerted on the probe while observing AFM images at high speed. This setup not only improves the accuracy of nanomanipulation but also enhances the operator's sensory experience, allowing for more intuitive and effective control during operations(Fig. S1, Fig. S2).

The initial background for AFM imaging in the environment is established as the baseline and is continuously updated locally based on this pre-acquired foundation. The operational system's local scan feature utilizes adaptive scanning patterns (such as raster or spiral) to detect the new position of a nano-object. This adjustment is enabled by accurately recovering the target's actual position through the measurement of height profiles. For example, the apex of a particle can be quickly identified by employing a spiral scanning pattern near the particle to observe its height profile. This method allows for the rapid recovery of the true position of nanoscale objects, typically in less than 100 milliseconds. Subsequently, a new global image can be produced, incorporating compensation for any new local imaging errors, as illustrated in Fig. 5. This process ensures highly accurate and timely updates to the imaging data, crucial for effective nanoscale manipulation and analysis.

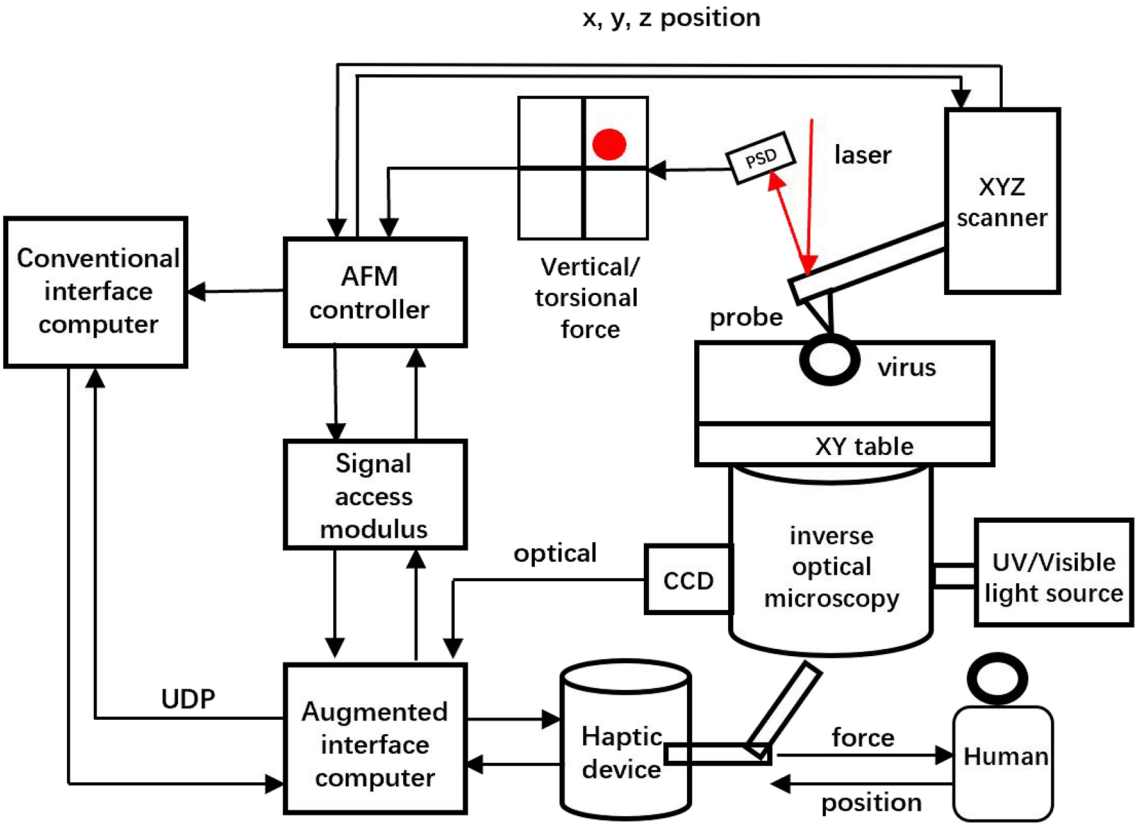

Fig. 4 Structure of nanorobotic system

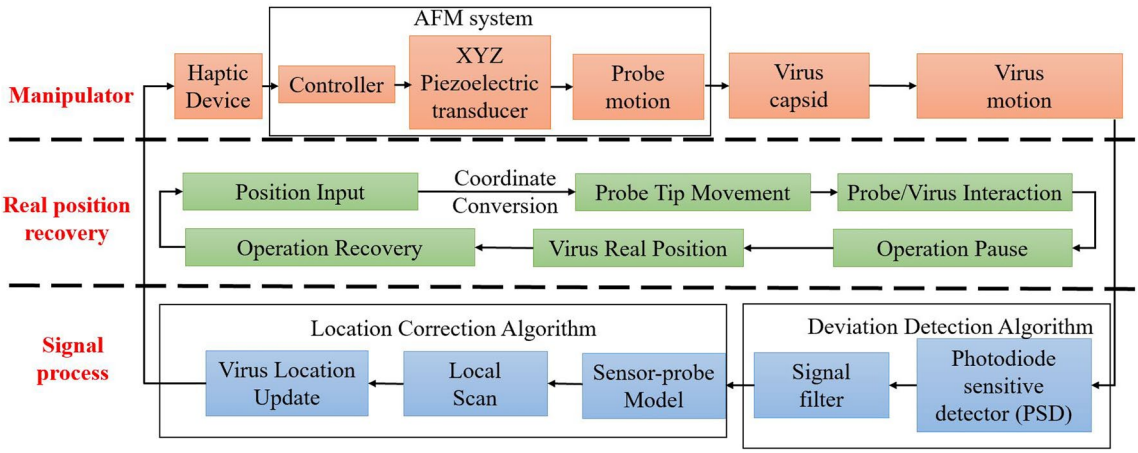

Fig. 5 Flowchart of virus capsid manipulation scheme by nanorobotic system

3.2 Condition judgement by tip-cantilever force sensing

The force sensing capability of system is intrinsically linked to the design of the probe-tip structure as well as the efficiency of the laser reflection system. Crucial to this process is the calculation of the sensitivity factor, which enables the conversion of sensor voltage readings (taken at the deflection output of the measuring electronics) into the actual deflection distance of the cantilever tip in nanometers. The beam deflection method is employed by the majority of AFMs. This involves directing a laser beam from a diode onto the end of the cantilever's backside.

The beam is reflected off the cantilever into a photodiode array. However, the absolute intensity captured by the photodiode can vary due to fluctuations in laser power or changes in the laser beam's focus on the cantilever [30]. To be independent of the signal's absolute strength, the normalized intensity of the four photodiodes have been measured, while the vertical signal and lateral signal could be calculated by the algorithm of four photodiodes. The contact force is applied to the AFM probe following Hooke's law $F = k * x$, with the function of probe deflection D, stiffness of the probe k, and the sensitivities of PSD signals from probe deflection (Fig. 6):

The initiation of position recovery is governed by the contact dynamics between the probe tip and the virus, characterized by four principal force transitions throughout the manipulation or disassembly procedure. The initial transition arises as the probe makes contact with the substrate-a process termed engagement. Subsequently, the probe's contact with the target object marks the second transition. A minor PSD shift follows, signifying the object-tip separation. Concluding the sequence, the probe's retraction occurs after an attempted motion, reverting the PSD to its baseline state, a process captured in Fig. 7.

The trigger of the contact and separation is depend on the lateral PSD signals, which could derive directly from the system, the correlation of the lateral force and PSD lateral signal is stated as:

$$S_L = \frac{F_L}{D_L K_L} \tag{6}$$

where the S_L is the PSD lateral signals and D_L is the system deflection sensitivities and the K_L is relative stiffness in lateral direction, the contact judgement is decided by the maximum slide force f_s or maximum rotation force f_r by the virus capsid [31]. The value of the trigger is pre-determined according to the test results. the η is coefficient of trigger and is usually set as 0.5 to ensure the accurate recognition and S_{Li} is the lateral PSD signal after engagement:

$$S_L \geq \eta * max\left(\frac{f_s}{D_L K_L}, \frac{f_t}{D_L K_L}\right) + S_{Li} \tag{7}$$

The separation force which is significantly less substantial than the contact force, presents a modeling challenge due to the intricate nature of interactions at the nanoscale. To accommodate this, the setpoint for force detection is empirically established through preliminary testing tailored to each unique experimental configuration, generally involving a voltage shift of no more than 50 mv.

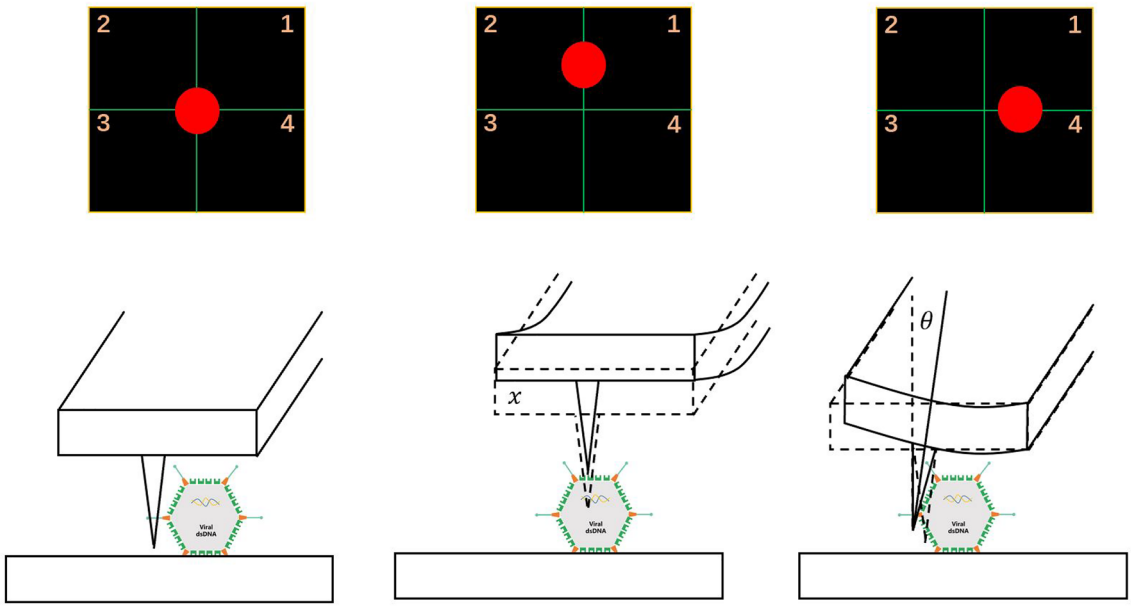

Fig. 6 Schematic of AFM probe PSD signal shift under different interaction conditions

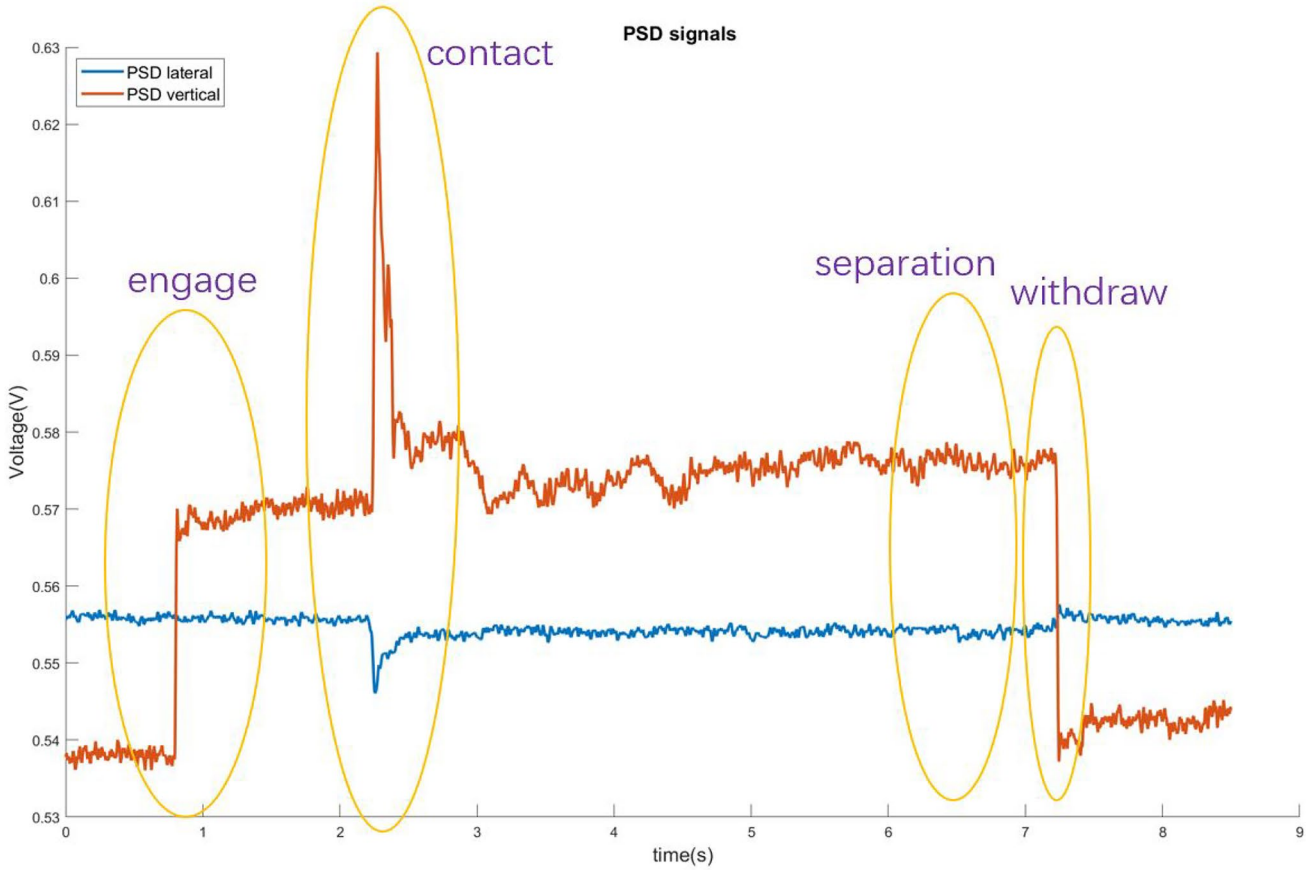

Fig. 7 PSD shift during the nano manipulation operation with four main shifts: engagement, contact, separation of sample-tip and withdraw of probe

3.3 Nanorobot manipulation scheme for virus capsid

Perform the interleaving local recovery algorithm, manipulation outputs can be updated in real-time within the operation interface. This entire adaptive close-loop manipulation operation is executed through the synchronous functioning of local position recovery and manipulation commands, with action times clocked under 100ms. Due to the high frequency of switching between operation and recovery, these processes become almost imperceptible to the user. Consequently, nanomanipulation that incorporates the recovery algorithm is significantly more reliable and experiences fewer operational failures. In the context of virus manipulation with a local-recovery-after-operation approach, a particle is repositioned from one spot to another, taking cues from local scan experiment results. This action prompts the generation of a specific scanning pattern and path, as depicted in Fig. 8. The use of local scan recovery negates the need for global mapping during the operation, which typically incurs a delay of several minutes to obtain fine images. The operational procedure can thus be succinctly described as an 'action-trigger-recovery-action' loop, enabling swift and precise manipulations within the nanoscale environment.

The interaction of the virus and probe could be adjusted in real time without refreshing the global images. The real position of the virus may be easily reconstructed from the local scan data using the particle center, which can be defined by the local scan. The developed system possesses the capability of accurately manipulating/disassembling the virus capsid.

The selection of imaging pattern is a significant parameter for the local scan performance. Raster scans often encounter issues with excessive motion due to abrupt stops and changes in direction. This imaging pattern minimizes overshoots and distortions in the collected data caused by sudden positional changes. In contrast, the spiral trajectory, being continuous and devoid of abrupt changes, results in smoother probe motion and prevents data and image distortion(Fig. S3). This pattern is particularly effective for spherical samples like viruses. The motion trajectory of the spiral scan is as follows:

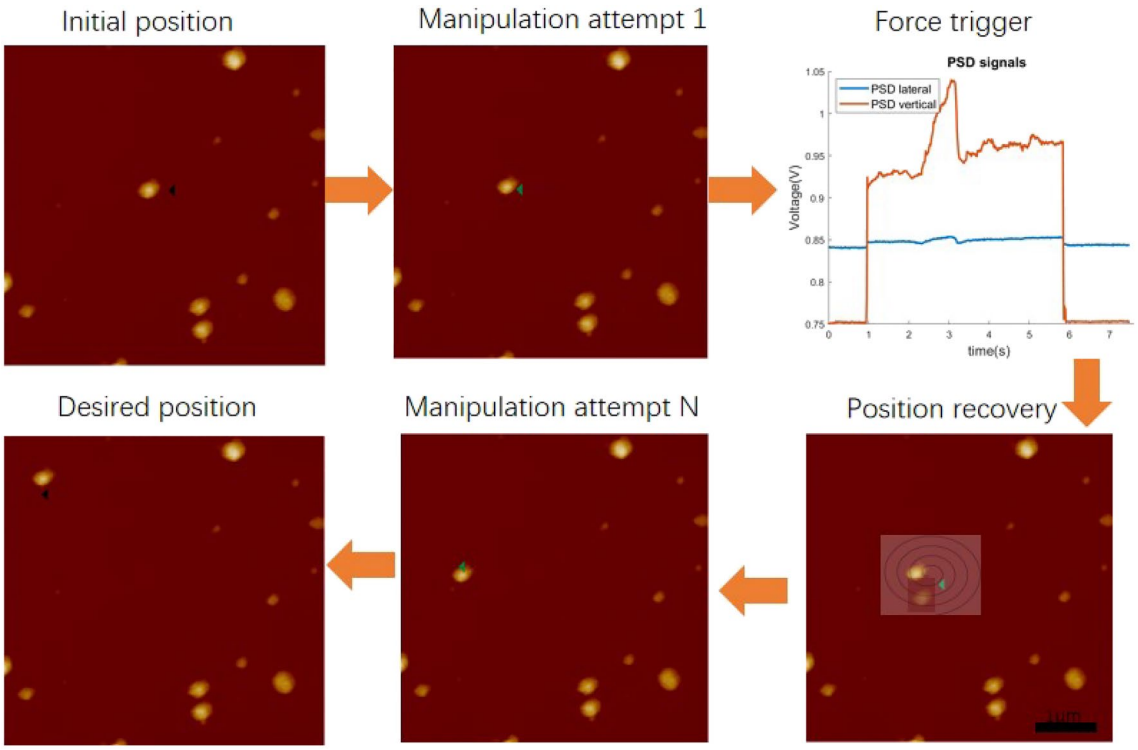

Fig. 8 Flow chart of position recovery during nanomanipulation

$$\begin{cases} x_i = (i-1)r_{step} * cos((i-1) * s_{step}) \\ y_i = (i-1)r_{step} * sin((i-1) * s_{step}) \end{cases} \tag{8}$$

Each spiral iteration increases the radius r_{step} based on the scan area, while the angle s_{step} increases incrementally. Additionally, each point generated during the iteration undergoes a distance threshold check to ensure that point spacing remains within a specified range. Regarding the scan area, we use a height threshold to distinguish the virus from the substrate, which helps determine the maximum scan range based on virus diameter. Typically, the scan area is set to 3-5 times the diameter of the virus to ensure accurate relocation. Since local scans primarily facilitate real-time observation of the virus's position, it is essential that the scan area includes the virus apex. The resolution of the local scan matches or exceeds that of the initial AFM scan image according to the adjustment of distance between sampling points.

4 Experimental setup and results

4.1 Experimental setup

Prior to conducting experiments with viruses, the system underwent rigorous testing to ensure accuracy and stability. Figure 9 illustrates the error between the haptic control input motion and the actual motion of the probe during operation, with the discrepancy between the haptic device and the probe's actual movement maintained below 0.5 pixel or less than 10nm in the physical world. In relation to 3D goggle usage, the close match between the Inertial Measurement Unit(IMU) signals received by the PC client and the original rotational data, along with the nano environment's rotation angle, reflects the video's adaptability to the operator's head movements. Figure 10 shows the operator's head angular velocity along the x and y axes with blue curve, and orange curves representing the angular velocity conveyed by the user interface to present the nanoscale environment. These results confirm that the AR feedback accurately mirrors the intended angular velocity, allowing the operator's view to shift in sync with their head movements, for deepening the sense of immersive operation.

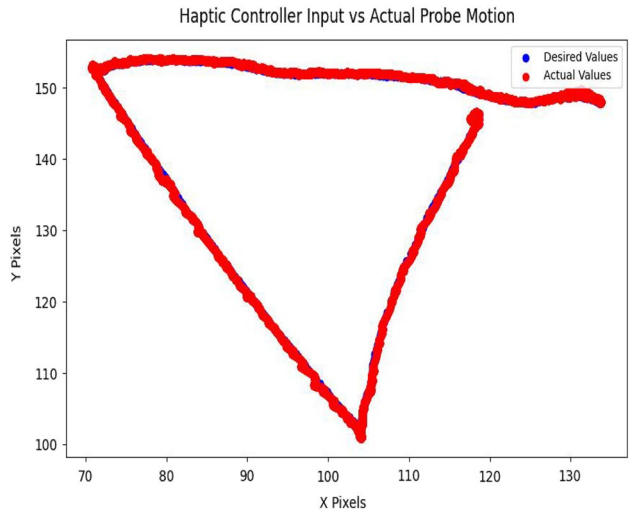

Fig. 9 Haptic controller input verses the actual probe motion for the probe operation

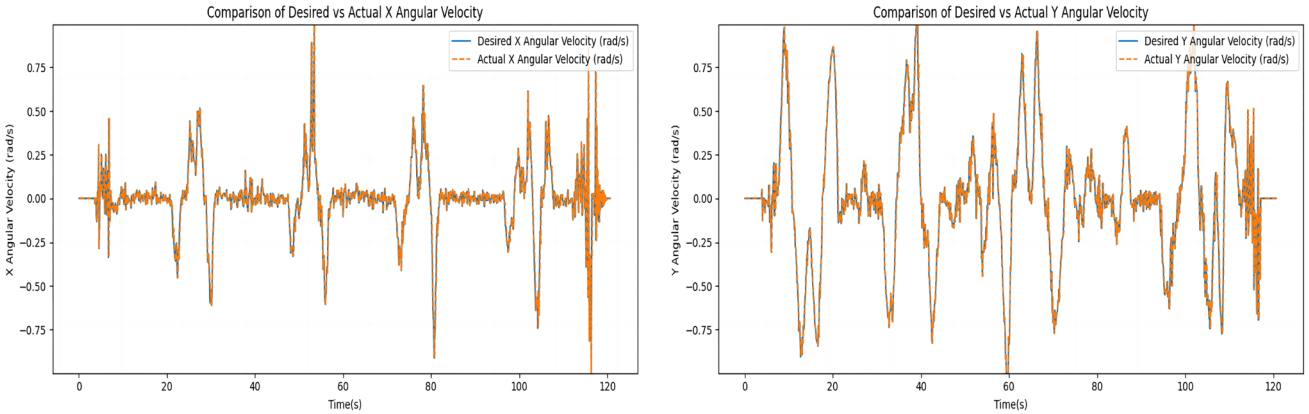

Fig. 10 Comparison of the desired X, Y angular velocity for the system and the actual 3D goggle headset measured angular

Green fluorescent protein transfected SARS-CoV-2 pseudovirus were prepared for the study (101bio, Inc). Before the AFM measurement, the mica substrate was first washed with acetone and then washed with DI water thoroughly. Then, 10 μ l virus solution was coated on the mica for 15 min, the substrate require certain hydrophilic ability to provide the virus capsid with firmly binding for scanning. After coating, the sample was dried out by the air after rinse. The two probes have been used in this experiment; the high-resolution imaging PEAKFORCE-HIRS-F-A probe (Bruker) with a stiffness of around 0.35 N/m has been selected; while for the manipulation and assembling experiment, the SCANANSYST-air probe with a stiffness of around 0.4 N/m has been selected, which have a larger contact region compared with the former one and pyramid probe with 20–60 nm spherical on the tip. During the experiement, the temperature is controlled as 20 °C by the heat panel beneath the substrate.

The images were recorded at a scan rate of 1 Hz, with a gentle applied force of around 500 pN, and the Peakforce tapping frequency of 2 khz with a resolution of 256 pixels^2. The scanning location has been selected with the image area varying from 5 to 1 μ m^2 to measure the different aspects of virus topography. Figure 11 shows the high-resolution topography of the virus capsid. The hexon shape protein fragments could be measured precisely, and the typical height of the virus capsid is between 60–80 nm, which represent the diameter of the virus, while the lateral measurement is larger than the height measurement due to the convolution effects. A similar imaging protocol is used for the following manipulation and assembling experiments.

4.2 Nanosurgery and manipulation of SARS-CoV-2 pseudovirus capsid

Following the imaging of virus capsids, a manipulation experiment was conducted to examine their interaction with inanimate surfaces and to assess their structural integrity. The probe's deformation was meticulously controlled to ensure

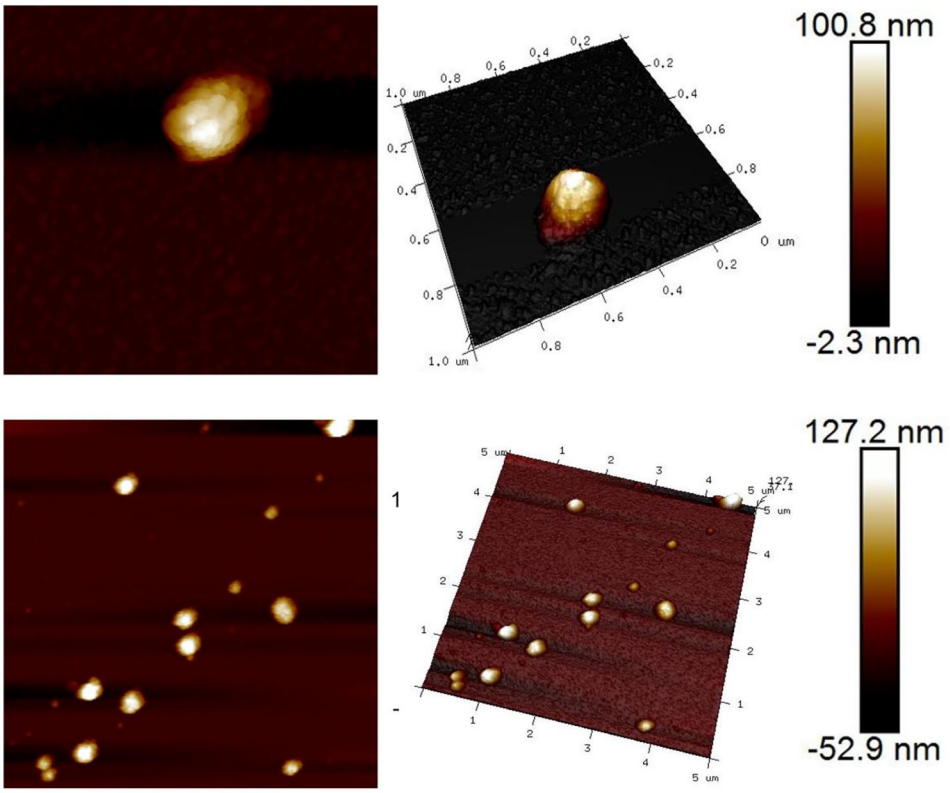

Fig. 11 High resolution 2D/3D topography of SARS-CoV-2 pseudovirus: top: scan size: 1 μ m^2; bottom: scan size: 5 μ m^2

only gentle contact with the substrate, exerting a vertical force ranging from 2 to 5 nN. This approach minimized lateral friction between the probe and the substrate. Employing the previously outlined manipulation algorithm, the virus was maneuvered across a distance of 5 μm, requiring fewer than 10 cycles of the 'action-trigger-recovery-action' sequence, as illustrated in Fig. 12A. The necessary force to detach the probe and the virus from the substrate's adhesion was approximately 10nN, as indicated in Fig. 12C. These results affirm that the nanorobotic system can effectively manipulate the virus capsid, thus shedding light on the nature of the interactions between the virus and inanimate surfaces.

The structural integrity of the SARS-CoV-2 virus under external stimulation was assessed by positioning the probe at the apex of the capsid and applying vertical movement along the virus's structure. When a force of 2 nN was exerted on the capsid, break events were recorded at forces ranging from 1 nN to 1.8 nN. The experimental data revealed a consistent decline in the interacting force as it progressed towards the base of the capsid, as depicted in Fig. 13.

To successfully dissect a virus capsid with a weak substrate-binding capacity, precise control over the initial positioning of the probe is crucial. The probe should engage the capsid laterally to minimize unnecessary sideways movements. The cutting process is then carried out with deliberate slowness, with the operator closely monitoring the PSD signals. Dissection continues until the vertical PSD signal reverts to its baseline value, indicating the completion of the cutting.

Following the dissection with the AFM probe, the resultant topography of the virus capsid was imaged, revealing a collapsed structure due to the cutting, as depicted in Fig. 12B, D. The central height of the capsid reduced from 65.4 to 51.2 nm. Surrounding the capsid were scattered protein fragments, with a measured height ranging from 8 to 12 nm. These measurements suggest that the capsid primarily consists of small protein fragments with an average thickness of approximately 10 nm, as illustrated in Fig. 14.

5 Discussion and conclusion

The utilization of atomic force microscopy as a tool for nanomanipulation has been broadly used in biological field over decade since the system doesn't require extra treatment to the targets to prevent the artefacts and damage during operation. However, convention AFM system has the limited capability to provide realtime visual feedback (requires fully scanned images) and lacks of closed-loop control during manipulation has impeded its widespread

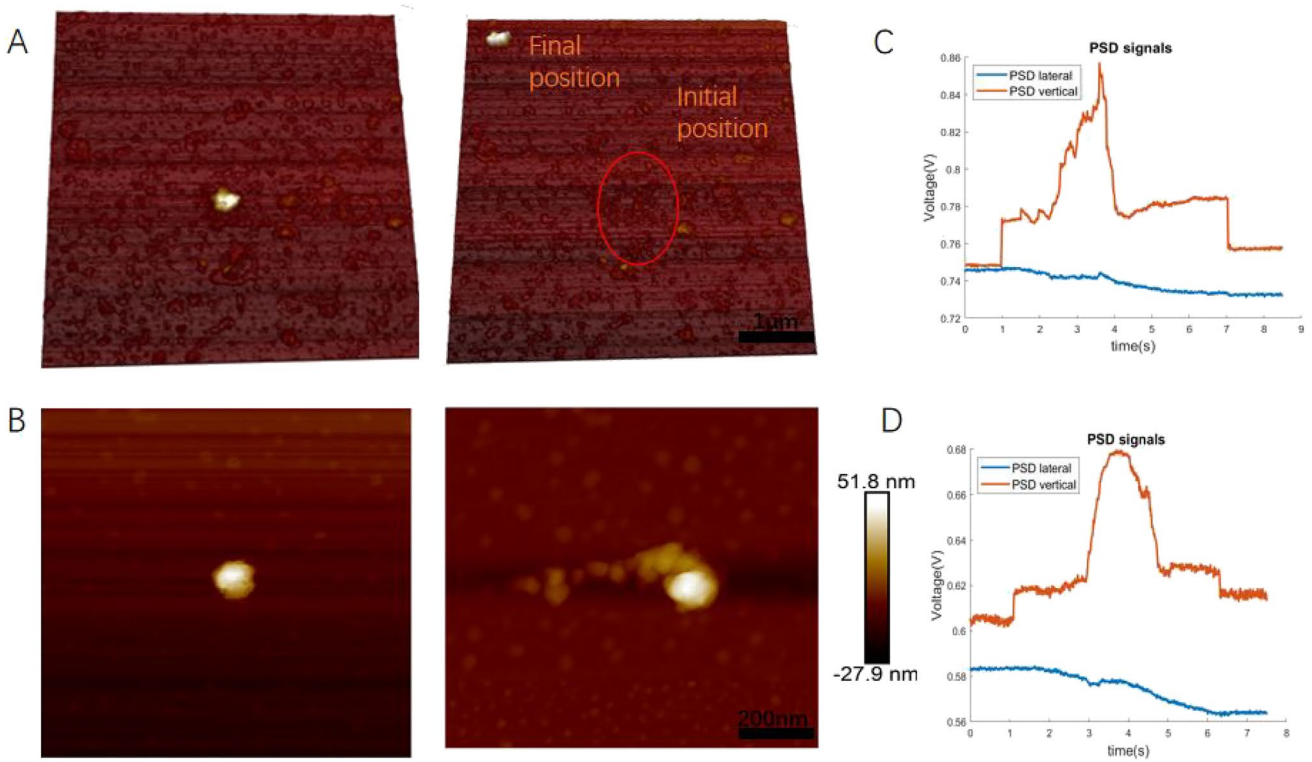

Fig. 12 AFM topography of SARS-CoV-2 pseudovirus capsid after nanorobot operation. **A** Left: Before the manipulation. Scan size: $5\mu m^2$; Right: After the manipulation Scan size: $5\mu m^2$. **B** Left: Before the disassembling. Scan size: $1\mu m^2$; Right: After the disassembling. Scan size: $1\mu m^2$. **C** PSD signal measurement for the manipulation of the virus capsid. **D** PSD signal measurement for the disassembling of the virus capsid

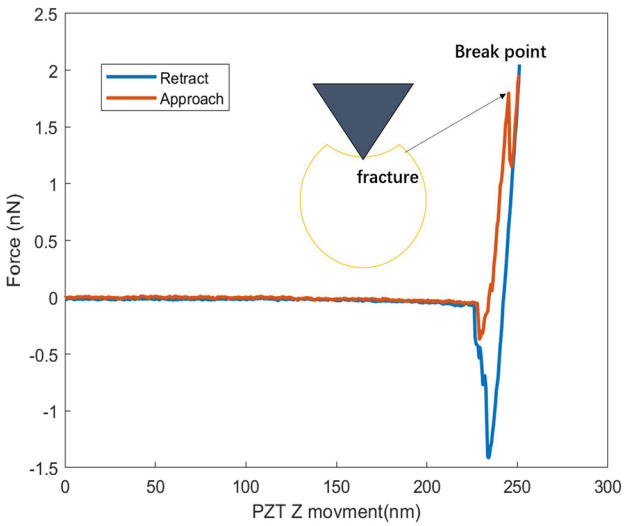

Fig. 13 Force-distance curve of vertical indentation on virus capsid apex until the fracture of the capsid. After the fracture point the force exerted on probe decreased instantaneously

application. The development of enhanced AFM-based nanorobotic system has adopted augmented reality system to overcomes this challenge by locally updating the AFM image in response to real-time force information during manipulation. In the delicate manipulation operation such as viruses surgery, the force applied to the probe usually maintained as hundred piconewton to few nanonewton, the haptic controller could generate human perceptible force to the operator. The stereoscopic vision further strengthen the accuracy and comfort level for the operator. In the aspect of closed-loop nanosurgery and manipulation task, the force-trigger based automatically control enable the realtime compensation of position error, the success rate is significant increase compared with the open-loop operation. The enhanced AFM system endow AFM-based nano-surgery and manipulation to the intelligent and

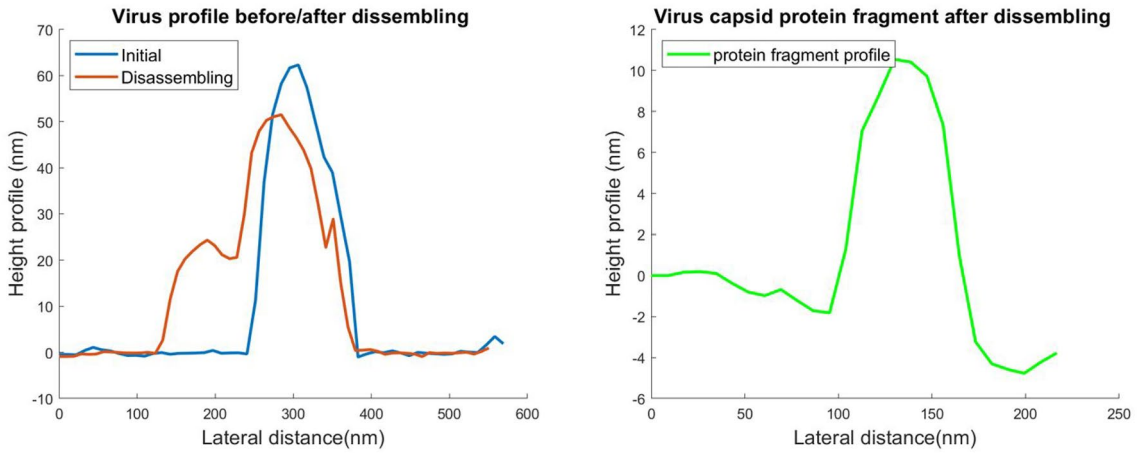

Fig. 14 AFM height profile: Left: virus initial/after disassembling height across the apex; Right: virus capsid protein fragment

efficient level, the once considered intricate operation in nanoscale become feasible to the operator to perform various of complex tasks.

In this study, a stereoscopic vision-based augmented reality system was presented, along with a force-triggered local recovery approach to eliminate manipulation errors during operations. The proposed system and algorithm facilitated the manipulation and disassembly of SARS-CoV-2 pseudovirus capsids. The AFM-based nanorobotic system demonstrated precise operation capabilities with high frame rates and imaging refresh rates (30 ms). By leveraging augmented reality technology and a position recovery scheme, the once laborious scanning scheme was effectively enhanced with local imaging, while probe actions were controlled through closed-loop compensation for highly accurate manipulation. In the field of virology investigation, the manipulation of the virus using this system revealed the weak binding between the virus capsid and inanimate surfaces. The disassembling results provided insights into the fracture process of the virus capsid under external forces, demonstrating that the protein capsid consists of several fragments of a protein complex with an approximate thickness less than 10 nanometer which provide the evidence for the structural measurement to the virus capsid. The experimental system and algorithm presented in this research serve as fundamental research tools and provide guidance for a deeper understanding of the structural mechanisms in viruses and other nanoscale targets which is important in the pharmaceutical industrial.

Author Contributions All authors contributed to the study conception. system integration, data collection and analysis were performed by Yuxuan Xue, Yichen Wang, Xinyu Liu and Jianfeng Liu. The first draft of the manuscript was written by Yuxuan Xue, Yichen Wang and Zhiyong Sun. The supervision and review was done by Jiangcheng Chen and Ning Xi. All authors read and approved the final manuscript.

Funding The work is partially supported by the CRF (C7174-20G), and GRF (17209521, 17212922), Hong Kong SAR, China. JCYJ20180504170303184, JCYJ20190806172007629 by Basic Research Program of Shenzhen, China, and Guangdong Basic and Applied Basic Research Foundation(2021A1515011423).

Data availability The datasets generated during and/or analysed during the current study are available from the corresponding author on reasonable request.

Declarations

Competing of interest The authors declare no conflict of interest.

References

1. Sharafi SM, Ebrahimpour K, Nafez A. Environmental disinfection against covid-19 in different areas of health care facilities: a review. Rev Environ Health. 2021;36(2):193–8.
2. Metcalf P, Cyrklaff M, Adrian M. The three-dimensional structure of reovirus obtained by cryo-electron microscopy. EMBO J. 1991;10(11):3129–36.
3. Ma Y, Xi N, Xue Y, Wang S, Wang Q, Gu Y. Development of a uvc-based disinfection robot. Indus Robot Int J Robot Res Appl. 2022;49(5):913–23.
4. Roos W, Bruinsma R, Wuite G. Physical virology. Nat Phys. 2010;6(10):733–43.
5. Timmermans SB, Hest JC. Self-assembled nanoreactors based on peptides and proteins. Curr Opin Colloid Interface Sci. 2018;35:26–35.
6. Dai X, Li Z, Lai M, Shu S, Du Y, Zhou ZH, Sun R. In situ structures of the genome and genome-delivery apparatus in a single-stranded RNA virus. Nature. 2017;541(7635):112–6.
7. Liu F, Liu X, Huang Q, Arai T. Recent progress of magnetically actuated DNA micro/nanorobots. Cyborg Bionic Syst. 2022
8. Mateu MG. Mechanical properties of viruses analyzed by atomic force microscopy: a virological perspective. Virus Res. 2012;168(1–2):1–22.
9. Chircov C, Grumezescu AM. Microelectromechanical systems (mems) for biomedical applications. Micromachines. 2022;13(2):164.
10. Dufrêne YF, Ando T, Garcia R, Alsteens D, Martinez-Martin D, Engel A, Gerber C, Müller DJ. Imaging modes of atomic force microscopy for application in molecular and cell biology. Nat Nanotechnol. 2017;12(4):295–307.
11. Xia F, Youcef-Toumi K. Advanced atomic force microscopy modes for biomedical research. Biosensors. 2022;12(12):1116.
12. Snijder J, Uetrecht C, Rose R, Sanchez-Eugenia R, Marti GA, Agirre J, Guérin D, Wuite G, Heck A, Roos W. Probing the biophysical interplay between a viral genome and its capsid. Nat Chem. 2013;5(6):502–9.
13. Xue Y, Ma Y, Sun Z, Liu X, Zhang M, Zhang J, Xi N. Identification and measurement of biomarkers at single microorganism level for in situ monitoring deep ultraviolet disinfection process. IEEE Trans NanoBiosci. 2023.
14. Marchetti M, Wuite G, Roos W. Atomic force microscopy observation and characterization of single virions and virus-like particles by nano-indentation. Curr Opin Virol. 2016;18:82–8.
15. Binnig G, Quate CF, Gerber C. Atomic force microscope. Phys Rev Lett. 1986;56(9):930.
16. Wen Y, Lu H, Shen Y, Xie H. Nanorobotic manipulation system for 360 characterization atomic force microscopy. IEEE Trans Industr Electron. 2019;67(4):2916–24.
17. Li G, Xi N, Yu M, Fung W-K. Development of augmented reality system for afm-based nanomanipulation. IEEE/ASME Trans Mechatron. 2004;9(2):358–65.
18. Liu L, Luo Y, Xi N, Wang Y, Zhang J, Li G. Sensor referenced real-time videolization of atomic force microscopy for nanomanipulations. IEEE/ASME Trans Mechatron. 2008;13(1):76–85.
19. Song B, Sun Z, Xi N, Yang R, Cheng Y, Chen L, Dong L. Enhanced nonvector space approach for nanoscale motion control. IEEE Trans Nanotechnol. 2018;17(5):994–1005.
20. Hou J, Liu L, Wang Z, Wang Z, Xi N, Wang Y, Wu C, Dong Z, Yuan S. AFM-based robotic nano-hand for stable manipulation at nanoscale. IEEE Trans Autom Sci Eng. 2012;10(2):285–95.
21. Sitti M, Horiguchi S, Hashimoto H. Tele-nanorobotics 2-d manipulation of micro/nanoparticles using afm. In: 1999 IEEE/ASME International Conference on Advanced Intelligent Mechatronics (Cat. No. 99TH8399), 1999. p. 786–786. IEEE.
22. Horiguchi S, Sitti M, Hashimoto H. Investigation of virtual reality interface for AFM-based nano manipulation. IEEJ Trans Electron Inf Syst. 2000;120(12):1948–56.
23. Yuan S, Wang Z, Liu L, Xi N, Wang Y. Stochastic approach for feature-based tip localization and planning in nanomanipulations. IEEE Trans Autom Sci Eng. 2017;14(4):1643–54.
24. Kallem V, Dewan M, Swensen JP, Hager GD, Cowan NJ. Kernel-based visual servoing. In: 2007 IEEE/RSJ International Conference on Intelligent Robots and Systems, 2007. p. 1975–1980. IEEE.
25. Sun Z, Xi N, Xue Y, Cheng Y, Chen L, Yang R, Song B. Task space motion control for afm-based nanorobot using optimal and ultralimit archimedean spiral local scan. IEEE Robot Autom Lett. 2019;5(2):282–9.
26. Meyer TR, Ziegler D, Brune C, Chen A, Farnham R, Huynh N, Chang J-M, Bertozzi AL, Ashby PD. Height drift correction in non-raster atomic force microscopy. Ultramicroscopy. 2014;137:48–54.
27. Ohzawa I. Mechanisms of stereoscopic vision: the disparity energy model. Curr Opin Neurobiol. 1998;8(4):509–15.
28. Quant M, Elizalde H, Flores A, Ramírez R, Orta P, Song G. A comprehensive model for piezoceramic actuators: modelling, validation and application. Smart Mater Struct. 2009;18(12): 125011.
29. Croft D, Shed G, Devasia S. Creep, hysteresis, and vibration compensation for piezoactuators: atomic force microscopy application. J Dyn Syst Meas Control. 2001;123(1):35–43.
30. Kontomaris S-V. The hertz model in AFM nanoindentation experiments: applications in biological samples and biomaterials. Micro Nanosyst. 2018;10(1):11–22.
31. Sümer B, Sitti M. Rolling and spinning friction characterization of fine particles using lateral force microscopy based contact pushing. J Adhes Sci Technol. 2008;22(5–6):481–506.